FULL PAPER

ADVANCED FUNCTIONAL MATERIALS

Supramolecular Organization in Fluorene/Indenofluorene–Oligothiophene Alternating Conjugated Copolymers**

By *Mathieu Surin*, *Prashant Sonar*, *Andrew C. Grimsdale*, *Klaus Müllen*, *Roberto Lazzaroni*, and *Philippe Leclère**

A series of conjugated copolymers containing fluorene or indenofluorene units alternating with oligothiophene segments, with potential interest for use as the active layer in field-effect transistors, is investigated. Atomic force microscopy analysis of the morphology of thin deposits shows either the formation of fibrillar structures, which are the signature of long-range π stacking, or the presence of untextured aggregates, resulting from disordered assembly. These morphologies are interpreted in terms of the supramolecular organization of the conjugated chains. Molecular modeling simulations indicate that the commensurability between the lengths of the monomer units and the presence of alkyl side groups are the two key structural factors governing the chain organization into highly ordered assemblies. The most favorable structures are those combining fluorene (indenofluorene) units with unsubstituted bithiophene (terthiophene) segments.

1. Introduction

Copolymerization is an efficient route for generating functional high-performance polymer materials with defined properties. In the field of polymer semiconductors, depending on the target application, macromolecular engineering combines the use of specific conjugated units and control of the copolymerization parameters to fine-tune the optoelectronic properties. For instance, different conjugated moieties can be combined in order to select the bandgap value and therefore the emission color of the materials,[1] or to modulate the charge-transport properties in organic field-effect transistors (OFETs),[2] or electron-donor and electron-acceptor units can be copolymerized to allow efficient charge-separation processes for photovoltaic diode applications.[3]

In this context, copolymers or co-oligomers made of thiophene units and fluorene units are particularly appealing, as illustrated by the following examples: i) various combinations of fluorene and thiophene oligomer units produce highly luminescent materials of distinct colors (depending on the composition), which can be useful for full-color display applications;[1a,4] ii) thiophene–fluorene oligomer structures have been prepared, with outstanding FET characteristics (mobility and on/off ratio on the order of 0.1 $cm^2 V^{-1} s^{-1}$ and 10^5, respectively);[5] iii) alternating copolymers of a fluorene derivative and bithiophene have been tested as active layers in all-polymer transistor circuits fabricated by ink-jet printing, where the liquid crystallinity of the compounds permitted the orientation of the chains on a rubbed substrate, giving rise to interesting circuit properties.[6] Moreover, this combination in copolymers leads to an enhancement of both the thermal stability and the stability against oxidation compared to those of oligo- and polythiophenes (the prototype materials used in OFET technology[7]) and is therefore a step forward towards devices with increased lifetime and efficiency.[4–6,8]

Although the luminescence and charge-transport properties of the fluorene–thiophene copolymers have been studied and reported in detail,[1a,4–6,8] the solid-state organization of the polymer chains in these copolymers and the microscopic structure of thin films (i.e., two aspects that can have tremendous impact on the performance of the devices) have hardly been described. To the best of our knowledge, such data have only been reported for a few thiophene–fluorene co-oligomers.[5b] This paper aims at a general understanding of the microscopic morphology of thin deposits of copolymers of fluorene with thiophene derivatives. To attain this goal, models of the supramolecular organization of the polymer chains have been designed and tested against the microscopic morphology determined experimentally. This approach has also been applied to new polymer structures, i.e., indenofluorene–oligothiophene copolymers that have been designed and synthesized for use in FETs. The interesting feature of the indenofluorene-containing conjugated

[*] Dr. P. Leclère, M. Surin, Prof. R. Lazzaroni
Service de Chimie des Matériaux Nouveaux
Université de Mons-Hainaut
Place du Parc 20, B-7000 Mons (Belgium)
E-mail: philippe@averell.umh.ac.be
Dr. P. Sonar, Dr. A. C. Grimsdale, Prof. K. Müllen
Max-Planck-Institut für Polymerforschung (MPI-P)
Ackermannweg 10, D-55128 Mainz (Germany)

[**] The collaboration between Mons and Mainz is conducted in the framework of the InterUniversity Attraction Pole Program (PAI V/3) of the Belgian Science Policy Office. Research in Mainz is supported by the Deutsche Forschungsgemeinschaft (Schwerpunktprogramm Organische Feldeffekttransistoren SFB 625). Research in Mons is partly supported by the European Commission, the Government of the Region of Wallonia (Phasing Out—Hainaut), and the Belgian National Fund for Scientific Research FNRS/FRFC. M.S. acknowledges F.R.I.A. for a doctoral scholarship. P.L. is a Research Associate of F.N.R.S. (Belgium).

  DOI: 10.1002/adfm.200500241

ADVANCED FUNCTIONAL MATERIALS

polymers is that the relative orientation of the single bonds connecting the indenofluorene units to the oligothiophene units is parallel, which is more likely to favor straight polymer chain conformations compared to fluorene-containing counterparts, in which those single bonds form a 25° angle, possibly leading to coiled conformations.

The compounds studied are shown in Scheme 1. Our study relies on the investigation of solution-processed thin deposits by means of tapping-mode atomic force microscopy (TM-AFM), a technique allowing the unraveling of the microscopic morphology with lateral and vertical resolution of 1 nm and 0.1 nm, respectively. To understand the results in terms of assembly of the chains, molecular modeling simulations are carried out on stacks of a few chains (up to four chains). Molecular modeling provides penetrating insight into the interchain and inter-segment interactions, which allows an understanding of how the chains pack to give rise to the observed structures. This joint "AFM plus modeling" approach is applied first to fluorene–thiophene co-oligomers and copolymers. Then it is extended to indenofluorene–oligothiophene alternating copolymers, for which particular attention is paid to the influence of the molecular architecture, in terms of length ratio between the comonomers and substituent position.

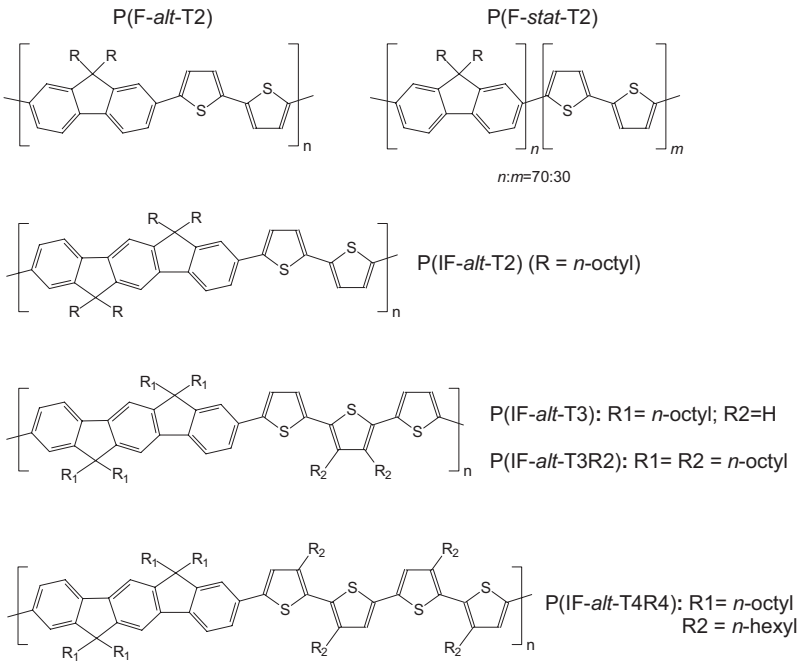

Scheme 1. Structures of the compounds studied. (Abbreviations: F, fluorene; T2, bithiophene; IF, indenofluorene; T3, terthiophene; T4, quaterthiophene.)

2. Results and Discussion

2.1. Copolymers of Fluorene and Bithiophene

The morphology of thin deposits of poly(9,9-dioctylfluorene-*alt*-bithiophene) (P(F-*alt*-T2), see Scheme 1) shows particular structures. For instance, in Figure 1a we observe a large object a few micrometers long (gray in the height image, the substrate being darker). The phase image (Fig. 1b) and the zoom images (insets) clearly reveal the internal structure, made of tortuous, interlaced, one-dimensional (1D) "fibrillar" structures. Even though the thickness of these structures seems to vary and is difficult to determine accurately (due to the fact that they are interlaced), image analysis reveals that these objects have similar dimensions in terms of width and height, i.e., they are between 25 and 40 nm wide and a few nanometers high. Finding these well-defined 1D structures, with such an aspect ratio, suggests that the chains are assembled into ordered aggregates.

Statistical copolymerization of fluorene and bithiophene offers the possibility of fine-tuning the bandgap of the compound, by controlling the ratio between the monomers. If this ratio is far from unity, the chain packing can be markedly different from that of alternating (50:50) copolymers. As an example, we examined the microstructure of such a copolymer, namely P(F-*stat*-T2), where the fluorene/bithiophene ratio is 70:30. The typical microscopic morphology of deposits of P(F-*stat*-T2) is shown in Figure 2. In both the height and phase images, bright objects are present on the substrate (appearing

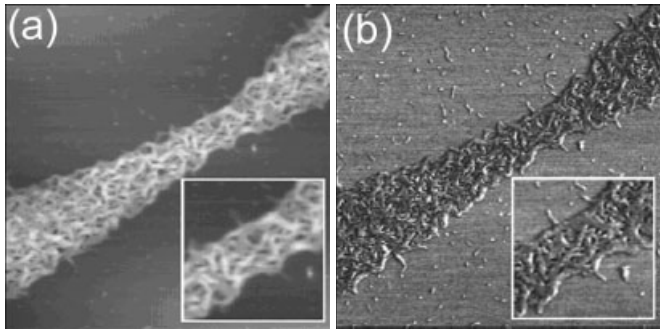

Figure 1. Tapping-mode AFM height (a) and phase (b) images (2.5 μm × 2.5 μm) of thin deposits of P(F-*alt*-T2) from tetrahydrofuran (THF) on mica. Insets: 750 nm × 750 nm images. The vertical grayscale of the height image is 10 nm.

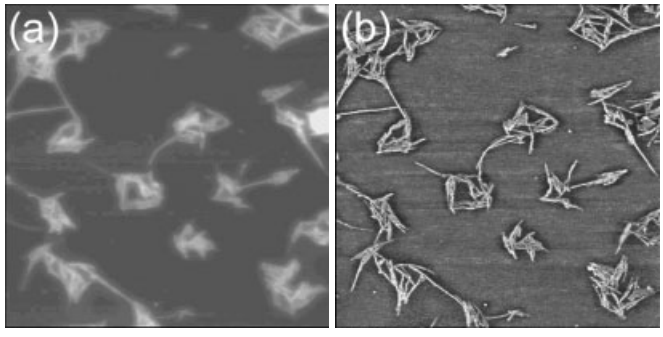

Figure 2. Tapping-mode AFM height (a) and phase (b) images (2.5 μm × 2.5 μm) of thin deposits of P(F-*stat*-T2) (F:T2 = 70:30) from THF on mica. The vertical grayscale of the height image is 10 nm.

darker). They are loose aggregates of straight 1D objects of varying length, but with similar lateral dimensions. The width of these fibrils is around 20–25 nm, while their height is a few nanometers (2 ± 1 nm). The deposits of polymers P(F-*alt*-T2) and P(F-*stat*-T2) thus display the same type of 1D structures with similar aspect ratio. Such fibrillar structures in thin deposits of conjugated polymers have been previously shown to result from the intrinsic self-assembly of planar conjugated chains, for example, poly(*p*-phenylene ethynylene)[9] and poly(9,9-dialkylfluorene),[10] due to favorable π–π interactions between the conjugated segments. In such structures, the conjugated main-chain axis is perpendicular to the stacking direction (the fibrillar axis), with the conjugated planes parallel to each other, edge-on over the substrate. Our AFM data support such a model of packing in the present case, since the width of the fibrils is consistent with the estimated average length of fully extended chains (estimated from the number-average molecular weight $\langle M_n \rangle$ obtained by gel permeation chromatography (GPC) using poly(*p*-phenylene) standards). With values of 10 420 g mol^{-1} and 7420 g mol^{-1} for P(F-*alt*-T2) and P(F-*stat*-T2), respectively, we estimate a contour length (fully extended configuration) of roughly 30 nm for the former and around 20 nm for the latter. These estimates are in good agreement with the measured widths of the fibrils: 25–40 nm and 20–25 nm for P(F-*alt*-T2) and P(F-*stat*-T2), respectively. Such an agreement indicates that these compounds form the same type of stacking within the fibrillar structures as homo-polyfluorene. The thickness of the fibrils (around 2 nm) is also consistent with the plane of the conjugated backbone oriented edge-on over the substrate and alkyl side groups of the fluorene units roughly in an extended configuration. Note that, while such fibrillar structures have already been observed for conjugated homopolymers, this is, to the best of our knowledge, the first such observation for copolymers made of different conjugated units.

The AFM data suggest that the chains are assembled with their axis perpendicular to the stacking direction (i.e., fibrillar axis). However, the relative positions and interactions of the different monomer units within a given chain with the adjacent ones remain unclear. To shed light on that question, we have applied molecular mechanics simulations to stacks of chains, in order to determine the molecular configurations adopted within the stacks, and the specific inter-segment interactions. These simulations use a set of energetic parameters (called the force field) that represents the interactions between bonded atoms (bond distances, bond angles, torsion angles) as well as the interactions between non-bonded atoms (van der Waals', electrostatic). The calculations are aimed at finding the most stable conformations by energy minimization starting from several different, chemically sound initial situations. We have not considered the presence of the surface in the simulations because deposits prepared on different substrates (mica, graphite, silicon wafer) all show the same morphology, which suggests that the driving force for assembly is the molecule–molecule interactions rather than molecule–substrate interactions.

In a first step, we consider a (fluorene–bithiophene)$_2$, (F-T2)$_2$, segment in the linear configuration, i.e., where the bridging carbon of the fluorene unit is anti to the sulfur atom of the neighboring thiophene unit, and with the two sulfur atoms of the bithiophene unit also in the anti configuration (see Fig. 3). This linear configuration is the most stable, since the steric hindrance is reduced between hydrogen atoms on fluorene and thiophene units compared to the configuration where the bridging carbon atom of fluorene and the sulfur atom of thiophene are syn (which is a few tenths of a kJ mol^{-1} less stable). The simulation indicates that the different segments (i.e., dioctylfluorene and bithiophene) are planar, with a torsion angle of 20° between these segments. Note that, using the same approach, we find the torsion angle between fluorene units in a poly(dioctylfluorene) chain to be around 36°; this smaller torsion highlights the small steric hindrance between hydrogens on adjacent monomer units in (F-T2)$_n$ chains compared to (F)$_n$ chains. If a torsion angle of 0° in (F-T2)$_n$ is imposed, the structure is only 5.9 kJ mol^{-1} (1.4 kcal mol^{-1}) less stable than the optimized structure (torsion angle of 20°). It is therefore rather likely that the chains easily adopt a fully planar configuration in the solid state to maximize the interchain interactions.

Based on that assumption, stacks of two planar (F-T2)$_2$ molecules were built in a cofacial configuration, as depicted in Figure 3a (where the fluorene and bithiophene segments are positioned in front of the same segment in the adjacent chain). The fluorene moieties facing each other on adjacent chains have their bridging carbon atoms pointing in opposite directions, which appears to be a stable configuration in stacks of homo-polyfluorenes.[10c] The equilibrium interchain distance is found to be around 0.45 nm, a typical value for stacks of planar aromatic chains.[11] The total energy of the system versus the relative displacement of one chain along the main-chain axis is shown at the top of Figure 3. Four stable structures (i.e., four minima, designated a, b, c, d) are found; they are shown at the bottom of Figure 3 (the conjugated backbones are parallel to the view, in different colors). When comparing structures a, b, c, d, we observe that all these stable configurations correspond to a strong overlap between conjugated rings, as a thiophene ring matches well the geometry of a benzene ring, and a bithiophene unit matches the geometry of a fluorene unit. The relative contributions of the non-bonding interactions (relative van der Waals' and electrostatic energies) are also displayed on the graph: minima a,c correspond to combinations of local minima in both contributions while minima b,d are due to electrostatic interactions only. The global minimum, conformation b, corresponds to a displacement along the *Z* direction of 0.42 nm (compared to the starting conformation a) and to the overlap of one bithiophene unit with one thiophene ring and one benzene ring of the adjacent chain. Conformation c (displacement of 0.84 nm along *Z*) corresponds to the overlap of fluorene units with bithiophene units. Note that the large increase in the relative total energy of the system when the displacement reaches 1.4 nm is due to the steric hindrance (van der Waals' interactions) between octyl substituents of adjacent fluorenes; this configuration is clearly unstable, and unfavorable interactions increase until the displacement along *Z* reaches 1.6 nm (not shown), where the substituted fluorenes overlap most strongly. Globally, the van der Waals' stabilization decreases (i.e., the corresponding energy increases) when the adjacent

ADVANCED FUNCTIONAL MATERIALS

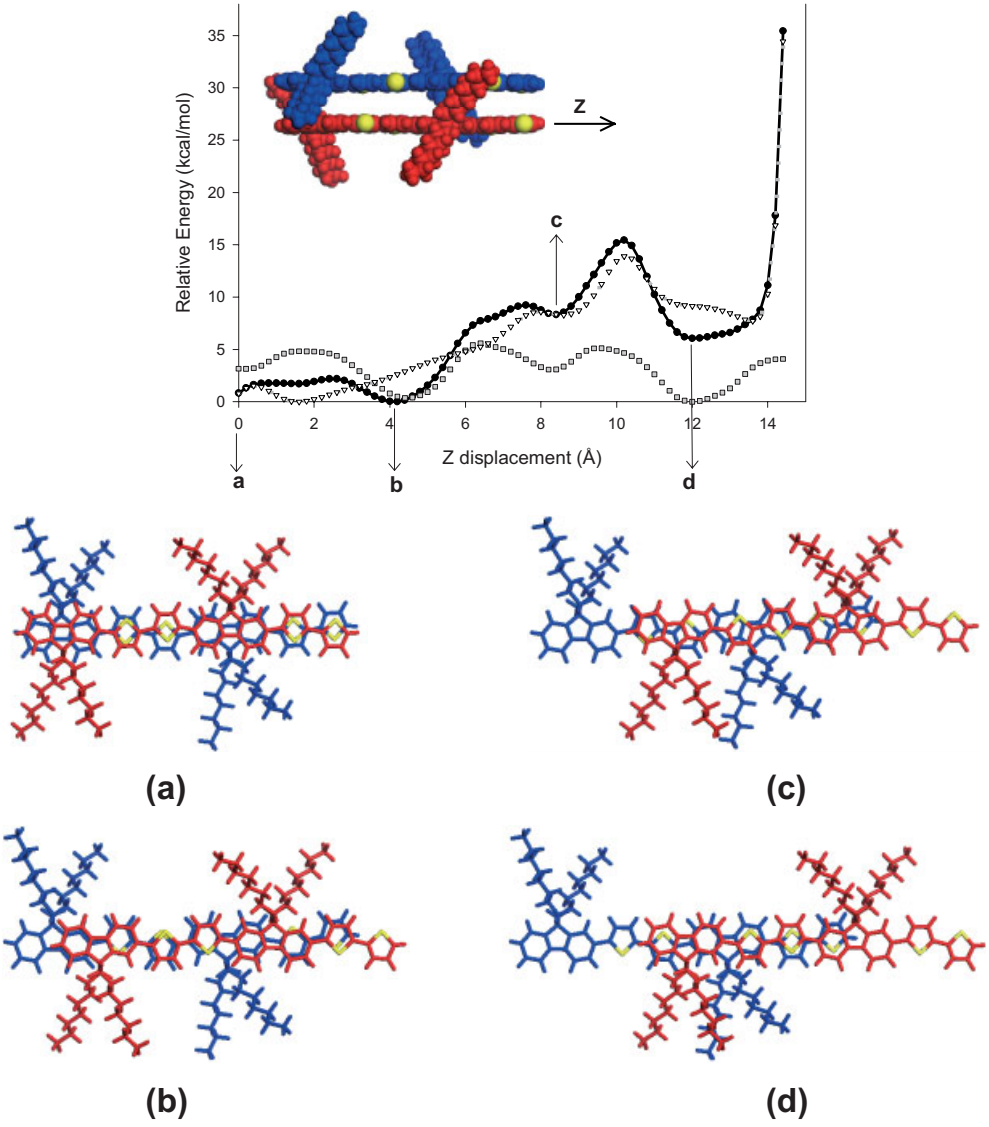

Figure 3. Molecular modeling of cofacial dimers $(F\text{-}T2)_2$ (interchain distance is 4.5 Å). Top: Graph showing the evolution of the relative total energy of the system (filled circles) versus the displacement along the *Z* direction. Contributions of the non-bonding interactions are shown as empty triangles (van der Waals') and gray squares (electrostatic). Bottom: Structures corresponding to the minima labeled a–d in the graph (the plane of the conjugated backbones is parallel to the view).

molecules are more displaced relative to each other, due to the decrease in the number of atomic van der Waals' contacts.

The observation of these stable configurations allows stable initial configurations to be selected for larger stacks, with longer chains: cofacial stacks of two to four hexamers $(F\text{-}T2)_6$ have been built based on these configurations. Interestingly, the most stable configuration (named conf1) for stacks of two $(F\text{-}T2)_6$ is found when the bithiophene units of one chain are located in front of the fluorene units of the other chain (equivalent to situation c in Fig. 3), at an equilibrium interchain distance d_{eq} of 0.44–0.45 nm. This structure is represented in Figure 4a, where the conjugated chains are shown perpendicular (left) and parallel (right) to the view. Compared to the other stable conformers obtained from different initial configurations, this most stable configuration is 62.7 kJ mol^{-1} (15.0 kcal mol^{-1}) more stable than the configuration where the bithiophene units of one chain are in front of one benzene ring and one thiophene ring of the adjacent chain (named conf2), and around 188 kJ mol^{-1} (45 kcal mol^{-1}) more stable than the configuration where the bithiophene units on one chain are in front of bithiophene units of the adjacent chain (named conf3). In the most stable configuration (conf1), the steric hindrance between substituents is minimal, because the octyl substituents on one chain are located in front of the unsubstituted bithiophene units on the next chain (Fig. 4a). Consistently, the equilibrium interchain distance d_{eq} increases on going from the most stable configuration ($0.44\ nm \leq d_{eq} \leq 0.45\ nm$) to conf2 ($0.47\ nm \leq d_{eq} \leq 0.48\ nm$) and conf3 ($d_{eq} > 0.5\ nm$). For a cluster of four $(F\text{-}T2)_6$ chains, the conf1 type of packing remains the most stable, with an interchain distance of 0.44–0.47 nm.

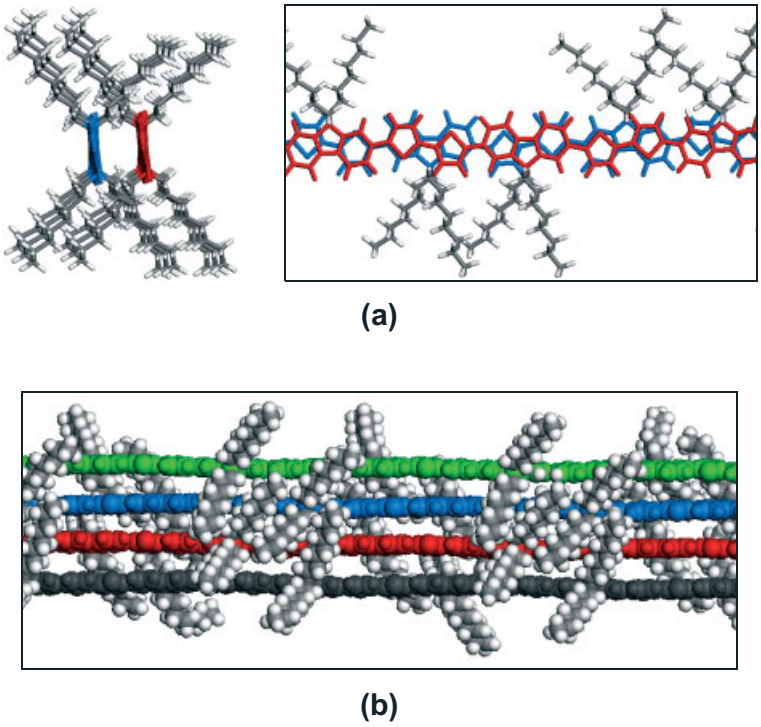

Figure 4. Molecular modeling of the assembly of a) two $(F\text{-}T2)_6$ chains, with the plane of the conjugated systems perpendicular (left) and parallel (right) to the view ("stick" representation), and b) four $(F\text{-}T2)_6$ chains, with the long axis in the plane of the view and the plane of the conjugated systems perpendicular to the view ("ball" representation).

The octyl substituents are extended in a quasi-perpendicular orientation relative to the long axis of the conjugated chain (see Fig. 4b), with very small steric hindrance between them. These results indicate that, in cofacial stacks of P(F-*alt*-T2) or P(F-*stat*-T2), bithiophene units of one chain have a strong tendency to be accommodated in front of fluorene units of the adjacent chain. This type of favorable π–π interaction will also take place when more copolymer chains join the stacks, thereby leading to 1D growth of π-stacked chains. This process eventually leads to the elementary fibrils observed in Figures 1,2. (The final aggregation of these fibrils into bundles of different shapes and sizes is probably controlled by the kinetics of solvent evaporation.)

2.2. Alternating Copolymers of Indenofluorene and Thiophene Oligomers

Alternating copolymers of tetraoctylindenofluorene (IF) with bithiophene or terthiophene (T2, T3, substituted or not, see Scheme 1) have also been studied. This series allows us to investigate the impact of i) the length ratio between the monomers and ii) the effect of the substitution patterns on the microscopic morphology. These polymers were synthesized as described in the literature,[12] which also reports on the relation between their optical, morphological, and electronic properties when used in FETs.

Thin deposits of P(IF-*alt*-T2) show a microscopic morphology of featureless aggregates or micrometer-sized solid droplets. The latter structures probably result from dewetting of small droplets during the formation of the deposit. No textured aggregates, which can be considered as the signature of long-range organization, were observed for this compound, suggesting that P(IF-*alt*-T2) chains cannot form dense π-stacked structures, in contrast to P(F-*alt*-T2). However, thin deposits of P(IF-*alt*-T3) on mica form specific structures (Fig. 5), with straight fibrillar assemblies growing over monolayer islands that have a constant thickness of 1.7 ± 0.2 nm. The fibrils are between 20 and 30 nm wide, and a few nanometers high (2.5 ± 0.5 nm, on top of the monolayers). The organization of the molecules into the monolayer is unclear (the height of the monolayers could be consistent with the molecules edge-on or tilted relative to the substrate plane). Since these monolayers are observed only on mica and not on the other substrates considered, they most likely result from a particular interaction with this substrate, while the fibrils, observed in all cases, result from intrinsic self-assembly of the polymer chains. The width of the fibrils is consistent with the formation of π stacks: considering that the degree of polymerization (determined from GPC with poly(*p*-phenylene) standards) is between ~7 ($\langle M_n \rangle = 6770$ g mol^{-1}) and ~13 ($\langle M_w \rangle = 12\,830$ g mol^{-1}), the length of the molecules in their fully extended configuration is between 17 and 31 nm, in very good agreement with the dispersity in the measured widths (between 20 and 30 nm).

To understand why P(IF-*alt*-T3) chains give rise to highly ordered π-stacked structures while P(IF-*alt*-T2) leads to untextured aggregates (despite their similar degree of polymerization), we applied molecular modeling. As observed in (F-T2) chains, the most stable configuration for (IF-T3) is when both bridging carbons of indenofluorene are anti to the sulfur atoms of the neighboring thiophene units, again with a torsion angle between the monomer units around 20°. Extending this configuration to a pentamer, with the oligothiophene segment in the anti conformation, leads to the structures shown in

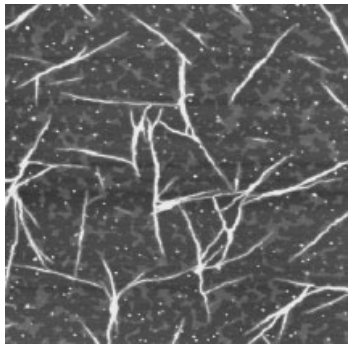

Figure 5. Tapping-mode AFM height image ($4.0\ \mu m \times 4.0\ \mu m$) of a thin deposit of P(IF-T3) from THF on mica. The vertical grayscale is 10 nm.

ADVANCED FUNCTIONAL MATERIALS

Figures 6a,b for $(IF\text{-}T2)_5$ and $(IF\text{-}T3)_5$, respectively. Note that these structures are shown fully planar for the sake of clarity; the most stable conformation actually corresponds to an alternation of torsion angles of +20° and –20° between thiophene and indenofluorene units. These results clearly show that the $(IF\text{-}T3)_5$ molecule is linear, while $(IF\text{-}T2)_5$ is significantly curved. This is due to a combination of geometric aspects: thiophene units are anti to the neighboring bridging carbon of the indenofluorene unit, combined with the fact that the S–C(thiophene)–C(indenofluorene) angle is around 120° and that neighboring thiophene units are in an anti configuration. Since it has been shown that a stable linear and planar configuration of the conjugated chains is necessary to obtain compact π stacking and consequently well-defined fibrillar structures,[9,13] it is anticipated that the assembly of P(IF-*alt*-T2) chains can hardly lead to such organized structures. To check this hypothesis, we performed modeling on stacks of two to four chains. For P(IF-*alt*-T3), stacks of pentamers were considered from different initial configurations where the steric hindrance is a minimum, as depicted in Figures 7a–c. The most stable configuration is found when the terthiophene segments of one chain are accommodated in front of the indenofluorene units of the other chain (Fig. 7d) at an equilibrium interchain distance of 0.46–0.47 nm. As can be seen on the left side of Figure 7d, the π systems of the two chains can efficiently overlap, giving rise to sizable π–π interactions. This opens the way to compact chain packing and ultimately to the formation of fibrillar structures. This situation, with an optimal "crossed" interchain overlap (i.e., between terthiophene segments on one chain and indenofluorene units on the other chain), is reminiscent of the case of P(F-*alt*-T2), where such overlap occurs between bithiophene segments and fluorene units. The "commensurability" between the comonomers (fluorene and bithiophene, indenofluorene and terthiophene) thus appears as a major geometrical feature promoting efficient intermolecular π–π interactions and consequently long-range π stacking. In contrast, in P(IF-*alt*-T2), no such dense packing can occur, because i) the chains are not linear and ii) in this case, a bithiophene segment can overlap only with two benzene rings of the indenofluorene unit. Modeling shows that the stacking of pentamers leads to structures where the chains are no longer in front of each other; instead they are displaced by a few tenths of a nanometer along the short axis of the conjugated chains (Fig. 8). The distance between the conjugated systems ranges from 0.6 to 1.0 nm. This large inter-

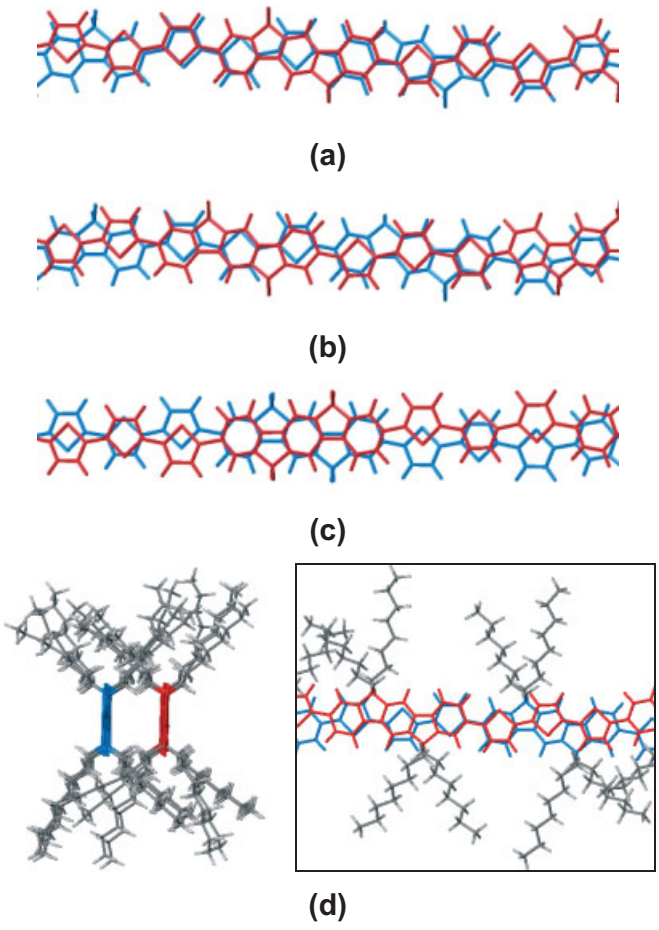

Figure 7. Molecular modeling of stacks of P(IF-*alt*-T3). a–c) Initial configurations (shown without substituents for the sake of clarity). d) View of the most stable configuration for stacks of two $(IF\text{-}T3)_5$ chains. ("Stick" representation, with the planes of the conjugated backbones shown parallel to the view, except for (d) left, in which they are perpendicular to the view.)

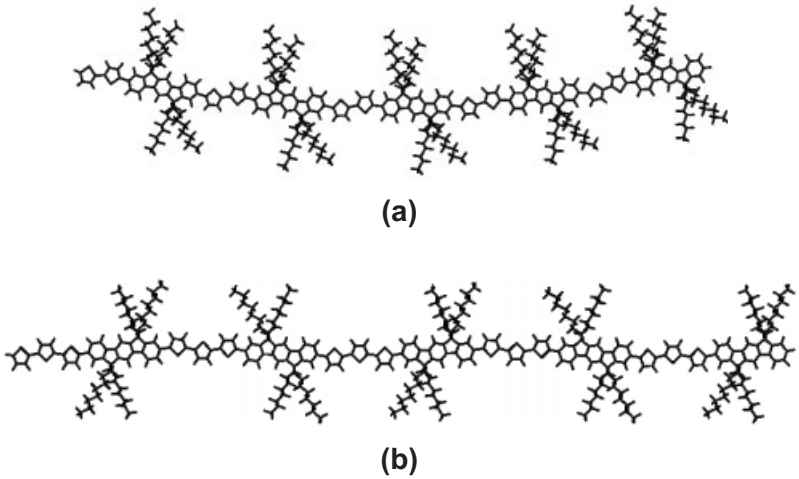

Figure 6. Molecular modeling of single chains of a) $(IF\text{-}T2)_5$ and b) $(IF\text{-}T3)_5$ ("stick" representation, with the plane of the conjugated backbone parallel to the view).

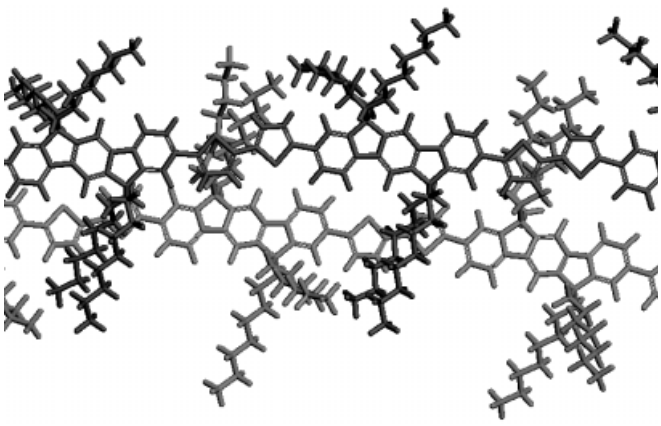

Figure 8. Molecular modeling of a stack of two $(IF\text{-}T2)_5$ chains. ("Stick" representation, with the planes of the conjugated backbones shown parallel to the view.)

chain distance and the non-cofacial configuration preclude any significant π–π interaction. As a consequence, compact π stacks are unlikely to form, which is consistent with the fact that thin deposits of P(IF-*alt*-T2) do not show well-organized fibrils but rather untextured aggregates.

To examine the effect of substitution on the terthiophene segment on the microscopic morphology, we designed P(IF-*alt*-T3R2), where two octyl groups are located on the central thiophene ring of the terthiophene segment. Thin deposits of this compound exhibit large flat islands (Fig. 9). The thickness of these layers is between 1.0 and 1.8 nm; these low values are typical of a monolayer, with the conjugated chains either edge-on perpendicular or tilted relative to the substrate plane. Nevertheless, these structures show no sign of long-range ordering. Since the thin deposits of P(IF-*alt*-T3) and P(IF-*alt*-T3R2) were prepared in the same way, the difference in terms of morphology is likely to be related to differences in chain packing, due to the difference in the substitution patterns: P(IF-*alt*-T3R2) has four octyl substituents on the indenofluorene units (these substituents are not in the plane of the conjugated system) and two substituents on a thiophene ring (these substituents can be in the plane of the conjugated system). If we assume that the indenofluorene and terthiophene units are coplanar, the alkyl groups on the former and on the latter would clearly be oriented in different directions, probably increasing the overall steric crowding, which would lead to a different type of packing than in P(IF-*alt*-T3). To check this hypothesis, we modeled stacks of P(IF-*alt*-T3R2), building pentamers in the same initial configurations as those depicted in Figures 7a–c. Note that the thiophene rings in the terthiophene segment remain coplanar, since substitution has no effect on the steric hindrance when the thiophene rings are in the anti conformation. In the most stable configuration for a two-chain cluster, two thiophene rings of the terthiophene segment are in front of two benzene rings of the indenofluorene unit of the adjacent chain (this configuration closely resembles that of Fig. 7a) with $d_{eq} \sim 0.47$ nm. The configuration where the terthiophene is fully overlapping with the indenofluorene unit (Fig. 7b) is 43.9 kJ mol^{-1} (10.5 kcal mol^{-1}) less stable (with $0.58\ \text{nm} \leq d_{eq} \leq 0.60\ \text{nm}$). In the four-chain cluster, the most stable configuration is not equivalent to that found for the two-chain cluster. Instead the substituted terthiophenes are in front of the indenofluorenes, as a result of steric hindrance constraints that are not present in the two-chain cluster. Most importantly, the equilibrium interchain distance is increased to 0.58–0.64 nm. Such a large value is no longer consistent with the formation of dense packing arising from π-stacked chains. Therefore, fibrillar structures are not expected to be formed in this case, highlighting the fact that the substitution patterns can have a huge influence on the chain packing of such copolymers, as already observed in indenofluorene homopolymers.[14] For P(IF-*alt*-T4R4), no fibrillar texture was observed, but rather untextured deposits as in P(IF-*alt*-T2) and P(IF-*alt*-T3R2). In P(IF-*alt*-T4R4), both the lack of "commensurability" between the comonomers (IF vs. T4) and the presence of substituents on thiophene rings prevent the assembly into regular π-stacked structures. Note that Liu et al. have shown that the position of the substituent on the (oligo)thiophene unit has a strong impact on the optical properties and conjugation length of fluorine–(bi)thiophene polymers.[4a] This, together with our results, highlights that the nature and position of alkyl substituents strongly influence the chain packing of such copolymers.

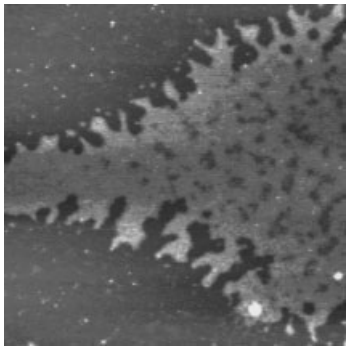

Figure 9. Tapping-mode AFM height image (3.0 μm × 3.0 μm) of a thin deposit of P(IF-*alt*-T3R2) from THF on mica. The vertical grayscale is 5 nm.

In a separate publication,[12] we will report that the morphology of thin deposits of these copolymers, reflecting the degree of long-range order in the chain packing, is correlated to their charge-transport properties in FETs. The compounds giving rise to a fibrillar morphology show better performances (higher charge mobilities and on/off current ratios) than those displaying disordered morphologies. Therefore, the study of the microstructure of thin deposits in combination with molecular modeling appears a useful tool for gaining insight into the structural order resulting from specific chain packing, which is expected to have a major effect on the performances of FET devices.

3. Conclusions

We have studied the microscopic morphology of thin deposits of copolymers of fluorene or indenofluorene with oligo(thiophene) units. From AFM investigations, we have

shown that, depending on the compound studied, highly regular fibrillar structures or disordered, untextured aggregates are formed. Comparison with molecular modeling indicates that the formation of these structures strongly depends on the molecular architecture: i) the nature and the "commensurability" between the different comonomers within the chains in alternating copolymers seems to be particularly important to achieve efficient π stacking: fluorene units tend to be accommodated in front of bithiophene segments, while indenofluorene units preferentially locate in front of terthiophene segments; ii) the number and position of the alkyl substituents have a strong impact on the assembly of the chains, since an increase in the overall steric hindrance disrupts the dense packing into fibrillar structures, which in turn is expected to strongly influence the optoelectronic properties.

4. Experimental

Synthesis: A detailed description of the synthesis of the indofluorene-containing copolymers is presented in a separate paper [12]. Poly(fluorene-*alt*-bithiophene) (P(F-*alt*-T2)) was prepared by the method of Leclerc and co-workers [1a].

Poly(fluorene-stat-bithiophene) (P(F-stat-T2)): A solution of $Ni(COD)_2$ (COD: cyclooctadiene) (446 mg, 1.67 mmol), 2,2′-bipyridine (262 mg, 1.67 mmol), and 1-5 cyclooctadienyl (180 mg, 1.67 mmol) in dry dimethylformamide (DMF, 10 mL) was stirred at 75 °C for 30 min under argon atmosphere. A solution of 2,7-dibromo-9,9-dioctylfluorene (384 mg, 0.70 mmol) and 5,5′-dibromo-bithiophene (98 mg, 0.30 mmol) in dry toluene (24 mL) was added, and the mixture was stirred at 75 °C for 72 h and then poured into a methanol (800 mL)/HCl (200 mL) mixture. The crude product was collected, dissolved in chloroform, and then reprecipitated from methanol. Reprecipitated polymer was again dissolved in chloroform and then washed with EDTA (ethylenediaminetetraacetate) solution to remove metal impurities. The low molecular weight fraction and residual impurities were removed by extraction with acetone in a Soxhlet apparatus to give the polymer (280 mg, 72 %). $M_n = 7400$ g mol^{-1}, $M_w = 22\,400$ g mol^{-1}, polydispersity index: 3.02 (polystyrene standards). ^{1}H NMR (250 MHz $CDCl_3$): δ [ppm] 7.90–7.20 (bm, 6H), 2.12 (m, 4H), 1.50–0.60 (m, 28H). ^{13}C NMR (62.5 MHz CD_2Cl_2): δ [ppm] 153.74, 152.23, 151.55, 140.87, 140.45, 126.49, 121.87, 120.34, 40.74, 32.16, 30.97, 30.37, 30.07, 24.32, 22.97, 14.21.

Molecular Modeling: Molecular mechanics calculations were performed using the Cerius2 and Materials Studio 3.0 packages developed by Accelrys. We used UFF 1.02 as the force field [15], since it properly describes the geometry of thiophene, fluorene, and indenofluorene. Atomic charges were assigned using the PCFF force field [16] and imported into the UFF calculations. Oligomers were built (from tetramers to hexamers) from coplanar monomers. Geometry optimization was performed until convergence was reached (using the conjugate gradient method, with the RMS force criterion set to 10^{-3} kJ mol^{-1} Å^{-1}). The long-range non-bonded interactions were calculated using the Spline method, with spline-on and spline-off parameters set to 1.1 and 1.4 nm, respectively. In the first step, stacks of two chains were built; four-chain clusters were then built, based on the optimized two-chain stacks, and investigated. Equilibrium distances between the chains were obtained by allowing the distance between the chains to evolve and the substituents to rotate during energy minimization. Several starting geometries and distances between backbones were tested. Zoa v2.0 software was used for visualization and data presentation [17].

Sample Preparation: For AFM investigations, all the samples were prepared in the same way: thin deposits were generated by solvent casting from THF or toluene dilute solutions (0.05–0.5 mg mL^{-1}) onto freshly cleaved muscovite mica substrates; the solvent was evaporated slowly at room temperature in a solvent-saturated atmosphere. The sample preparation conditions were chosen so that sub-monolayer deposits were formed, as we have observed previously [13] that the morphological analysis of such thin systems provides clearer information about chain assembly than studies on thicker layers.

Atomic Force Microscopy: Tapping-mode atomic force microscopy was performed with a Nanoscope IIIa microscope from Veeco (operating in air, 25 °C). The instrument is equipped with the Extender Electronics Module to provide simultaneously height and phase cartography. The latter corresponds to the measurement of the phase lag between the photodiode response and the excitation signal of the oscillating cantilever. It is particularly sensitive to small changes in the tip–sample interaction, thereby providing extra information on the morphology. Microfabricated silicon cantilevers with a spring constant of ~30 N m^{-1} were used. Images of different areas of the samples were collected with the maximum available number of pixels (512) in each direction. The Nanoscope III v5.12 image processing software was used for image analysis.

Received: April 20, 2005
Final version: May 31, 2005
Published online: July 26, 2005

[1] a) A. Donat-Bouillut, I. Lévesque, Y. Tao, M. D'Ioro, S. Beaupré, P. Blondin, M. Ranger, J. Bouchard, M. Leclerc, *Chem. Mater.* **2000**, *12*, 1931. b) C. Ego, D. Marsitzky, S. Becker, J. Zhang, A. C. Grimsdale, K. Müllen, J. D. MacKenzie, C. Silva, R. H. Friend, *J. Am. Chem. Soc.* **2003**, *125*, 437.

[2] a) M. Redecker, D. D. C. Bradley, M. Inbasekaran, W. W. Wu, E. P. Woo, *Adv. Mater.* **1999**, *11*, 241. b) S.-Y. Song, M. S. Jang, H.-K. Shim, D.-H. Hwang, T. Zyung, *Macromolecules* **1999**, *32*, 1482. c) T. Miteva, A. Meisel, W. Knoll, H. G. Nothofer, U. Scherf, D. C. Müller, K. Meerholz, A. Yasuda, D. Neher, *Adv. Mater.* **2001**, *13*, 565. d) C. D. Dimitrakopoulos, P. R. L. Malenfant, *Adv. Mater.* **2002**, *14*, 99. e) H.-F. Lu, H. S. D. O. Chan, S.-C. Ng, *Macromolecules* **2003**, *36*, 1543. f) P. Sonar, J. Zhang, A. C. Grimsdale, K. Müllen, M. Surin, R. Lazzaroni, P. Leclère, S. Tierney, M. Heeney, I. McCulloch, *Macromolecules* **2004**, *37*, 709.

[3] a) U. Stalmach, B. de Boer, C. Videlot, P. F. van Hutten, G. Hadziioannou, *J. Am. Chem. Soc.* **2000**, *122*, 5464. b) A. Marco, M. T. Rispens, J. K. J. van Duren, J. C. Hummelen, R. A. J. Janssen, *J. Am. Chem. Soc.* **2001**, *123*, 6714. c) H. A. M. van Mullekom, J. A. J. M. Vekemans, E. E. Havinga, E. W. Meijer, *Mater. Sci. Eng.* **2001**, *32*, 1.

[4] a) B. Liu, W. L. Yu, Y. H. Lai, W. Huang, *Macromolecules* **2000**, *33*, 8945. b) E. Lim, B. J. Jung, H. K. Shim, *Macromolecules* **2003**, *36*, 4288.

[5] a) H. Meng, Z. Bao, A. J. Lovinger, B. Wang, A. M. Mujsce, *J. Am. Chem. Soc.* **2001**, *123*, 9214. b) H. Meng, J. Zheng, A. J. Lovinger, B.-C. Wang, P. G. Van Patten, Z. Bao, *Chem. Mater.* **2003**, *15*, 1778.

[6] a) H. Sirringhaus, R. J. Wilson, R. H. Friend, M. Inbasekaran, W. Wu, E. P. Woo, M. Grell, D. D. C. Bradley, *Appl. Phys. Lett.* **2000**, *77*, 406. b) H. Sirringhaus, T. Kawase, R. H. Friend, T. Shimoda, M. Inbasekaran, W. Wu, E. P. Woo, *Science* **2000**, *290*, 2123.

[7] a) F. Garnier, R. Hajlaoui, A. Yassar, P. Srivastava, *Science* **1994**, *265*, 1684. b) G. Horowitz, *Adv. Mater.* **1998**, *10*, 365. c) H. Sirringhaus, P. J. Brown, R. H. Friend, M. N. Nielsen, K. Bechgaard, B. M. W. Langeveld-Voss, A. J. H. Spiering, R. A. J. Janssen, E. W. Meijer, P. Herwig, D. M. de Leeuw, *Nature* **1999**, *401*, 685.

[8] a) A. Charas, J. Morgado, J. M. G. Martinho, L. Alcacer, S. F. Lim, R. H. Friend, F. Cacialli, *Polymer* **2003**, *44*, 1843. b) M. Pasini, S. Destri, W. Porzio, C. Botta, U. Giovanella, *J. Mater. Chem.* **2003**, *13*, 807. c) Q. Hou, H. Niu, W. B. Huang, W. Yang, R. Q. Yang, M. Yuan, Y. Cao, *Synth. Met.* **2003**, *135*, 185.

[9] a) P. Samorì, V. Francke, K. Müllen, J. P. Rabe, *Thin Solid Films* **1998**, *336*, 13. b) P. Samorì, V. Francke, T. Mangel, K. Müllen, J. P. Rabe, *Opt. Mater.* **1998**, *9*, 390.

[10] a) J. A. Teetsov, D. A. Vanden Bout, *J. Am. Chem. Soc.* **2001**, *123*, 3605. b) J. Chappell, D. G. Lidzey, P. C. Jukes, A. M. Higgins, R. L. Thompson, S. O'Connor, I. Grizzi, R. Fletcher, J. O'Brien, M. Geo-

ghegan, R. A. L. Jones, *Nat. Mater.* **2003**, *2*, 616. c) M. Surin, E. Hennebicq, C. Ego, D. Marsitzky, A. C. Grimsdale, K. Müllen, J. L. Brédas, R. Lazzaroni, P. Leclère, *Chem. Mater.* **2004**, *16*, 994.

[11] See, e.g., U. H. F. Bunz, *Chem. Rev.* **2000**, *100*, 1605.

[12] P. Sonar, A. C. Grimsdale, K. Müllen, M. Surin, R. Lazzaroni, P. Leclère, J. Pinto, L.-L. Chua, H. Sirringhaus, R. H. Friend, unpublished.

[13] P. Leclère, E. Hennebicq, A. Calderone, P. Brocorens, A. C. Grimsdale, K. Müllen, J. L. Brédas, R. Lazzaroni, *Prog. Polym. Sci.* **2003**, *28*, 55.

[14] A. C. Grimsdale, P. Leclère, R. Lazzaroni, J. D. MacKenzie, C. Murphy, S. Setayesh, C. Silva, R. H. Friend, K. Müllen, *Adv. Funct. Mater.* **2002**, *12*, 729.

[15] a) A. K. Rappé, C. J. Casewit, K. S. Colwell, W. A. Goddard III, W. M. Skiff, *J. Am. Chem. Soc.* **1992**, *114*, 10 024. b) C. J. Casewit, K. S. Colwell, A. K. Rappé, *J. Am. Chem. Soc.* **1992**, *114*, 10 046.

[16] a) H. Sun, *J. Comput. Chem.* **1994**, *15*, 752. b) H. Sun, *Macromolecules* **1995**, *28*, 701.

[17] J. P. Calbert, *Zoa v.2.5*, Service de Chimie des Matériaux Nouveaux, Université de Mons-Hainaut, Mons (Belgium). http://zoa.freeservers.com.

